This article has been accepted for publication in a future issue of this journal, but has not been fully edited. Content may change prior to final publication. Citation information: DOI 10.1109/TPWRD.2018.2867851, IEEE Transactions on Power Delivery

A Fault Location Method for DC Lines Connected with DAB Terminal in Power Electronic Transformer

Shan Jiang, *Student Member, IEEE*, Chunju Fan, Ning Huang, Ye Zhu, Muwei He

***Abstract*--Power electronic transformer (PET) composed of modular dual active bridge (DAB) blocks has a promising future in AC/DC hybrid distribution network because of its energy routing ability. The key element that restrains the development of PET is the vulnerability of power electronic devices during faults, especially DC faults. DC faults (mostly line faults) have very short transient process and no obvious fundamental frequency, which means fault location is difficult to be realized for DC lines in distribution network. Considering that fault location plays an important role in realizing fast fault clearance and recovery, this paper analyzed fault characteristics of DC line faults with respect to the basic structure of modular DAB block and proposed a two-terminal fault location method based on transient voltages measured in DC line boundaries. To evaluate the validity of proposed method, numerical simulations with different fault conditions were implemented in PSCAD/EMTDC. The simulation results indicate that the proposed fault location method located the faulted point quickly and correctly.**

***Index Terms*--Dual active bridge (DAB), fault characteristic, fault location method, power electronic transformer (PET).**

I. Introduction

With the rapid development of semiconductor technology, power electronic devices have a wide and bright future in realizing more flexible control and more efficient transmission in power system. With increasing penetration of renewable energy, the converter configuration composed of VSCs or MMCs is widely applied in AC/DC hybrid power system [1], [2]. In recent years, a novel configuration of converter was proposed, which is based on modular dual active bridge (DAB) blocks [3], [4]. Its special structure brings an enhancement in power density, redundancy and modularity of transmission system [5]. The proposal of DAB-based converter configuration makes power electronic transformer (PET) come true, which is utilized to substitute for traditional AC transformer in distribution network.

The flexible connection and the multi-port characteristic of PET allows AC/DC hybrid and cascaded DAB structure realizes bidirectional energy conversion, which makes PET have potentials to be the most significant part in realizing energy Internet [6]. However, the biggest problem that restrains the development of PET is the vulnerability of power electronic devices with respect to potential faults, especially DC faults [7]. On the one hand, the technology of DC circuit breaker is still in progress and with high price. However, it has made some great progress in recent years with efforts of researchers around the world [8], [9]. On the other hand, fault characteristics of DC faults have very short duration but semiconductors in PET are under great threat during the fault, which means highly accurate fault detection and fault location methods should function with a shorter time window [10].

Considering that DC line faults account for a great proportion among DC faults, fault location method plays an important role in accelerating maintenance and reducing power outrage duration when DC line faults are detected. Hence, accurate fault location method brings great value to the reliability and stability of distribution network. For traditional AC system, numerous practical fault location methods have been proposed and they can be approximately divided into sequence-component-based method and traveling-wave-based method [11]-[14]. The sequence-component-based methods are apparently infeasible in DC system for lack of fundamental frequency [11]-[13]. Traveling-wave-based method was proved to be effective in locating faults for long distance cables in HVDC system [15], [16]. However, incredibly high sampling frequency (10 MHz) are required to locate fault for short cables in distribution network by this method [17], [18].

In recent years, some methods with different principles have been introduced to realize fault location in DC distribution network. During DC line faults, a probe power unit installed near the bus injects a probe current into the fault network after the trigger of DC circuit breaker and natural response of probe current reflects the fault location [19]. This method needs additional hardware unit and location accuracy is influenced by fault resistance. Although performance of this method has been improved in [20], maximum fault resistance considered in this paper is merely 2 ohms. A fault location method based on local measurement was proposed in [21], which relies on accurate current measurement. Yang et al. [22] proposed a method which realizes the fault location in pole-to-ground fault by solving a pair of equations related to terminal voltage and current. However, this method has a dead zone near the bus and complex solving process makes it unfeasible

Project Supported by National Key Research and Development Program (2017YFB0903201) of China.

The authors are with school of electronic information and electrical engineering, Shanghai Jiao Tong University, 200240 Shanghai, China (e-mail: jiangshan1995@sjtu.edu.cn).

0885-8977 (c) 2018 IEEE. Personal use is permitted, but republication/redistribution requires IEEE permission. See http://www.ieee.org/publications_standards/publications/rights/index.html for more information.

This article has been accepted for publication in a future issue of this journal, but has not been fully edited. Content may change prior to final publication. Citation information: DOI 10.1109/TPWRD.2018.2867851, IEEE Transactions on Power Delivery

to be applied in pole-to-pole fault.

Recently, J. Liu et al. [23] proposed a protection scheme for DC lines, which is based on the terminal inductor installed at each end of the DC line. This paper introduces a novel concept of ratio of transient voltage (*ROTV*), which is defined as the ratio of voltages measured at both sides of terminal inductor in frequency domain. *ROTV* defined in frequency domain shows a promising performance in DC line fault detection, but it is hard to be extended to fault location. Hence, this paper gives the definition of *ROTV* in time domain and realizes fault location with its time domain characteristics.

Since DC line fault is required to be isolated at the very beginning of fault for device protection, time window available for fault location is merely a few milliseconds [10]. What's more, performance of fault location will be influenced by operations of control system if time window is too large. The fault location method proposed in this paper overcomes the problem of time window and is practical for both pole-to-pole and pole-to-ground faults by utilizing *ROTV*s measured in line boundaries of two-terminal system.

This paper is organized as follows. In Section II, fault analysis of two common DC line faults with DAB terminal is discussed in detail with respect to fault distance and fault resistance. The concept of *ROTV* in time domain is introduced in Section III, which brings the basic principle of fault location method. In Section IV, the validity of proposed fault location method is tested under different fault conditions in PSCAD/EMTDC simulations. Furthermore, comparisons between proposed method and other methods are also presented in the last section.

II. Fault Analysis of DC Lines with DAB Terminal

A. Basic structure of PET

Fig. 1(a) displays a common structure of PET, which functions as the substation interfacing three different voltage levels. The interface between the MVAC and LVDC grid is realized by cascaded single phase converters and DABs. The modular structure of DABs makes the connection between grids with different voltage levels quite flexible. The interior structure of DAB is shown in Fig. 1(b), H-bridges at two sides of DAB ensure the feasibility of bidirectional energy conversion and the medium-frequency transformer realizes electrical isolation. When DC faults occur in the external lines of PET, fault characteristics only relate to H-bridges in DABs of fault side considering its special structure. Hence, short-circuit current and terminal voltage will be discussed based on the DAB structure.

B. Pole-to-pole Fault of DC Line

Pole-to-pole fault is considered as the most serious type in all DC line faults, which normally causes devastating consequences to the transmission system. For simplicity, P-N fault stands for pole-to-pole fault in the following paper. When pole-to-pole fault occurs in DC lines, IGBTs in DABs will be blocked immediately for self-protection with abnormal voltage or current detected. Nonetheless, anti-parallel diodes

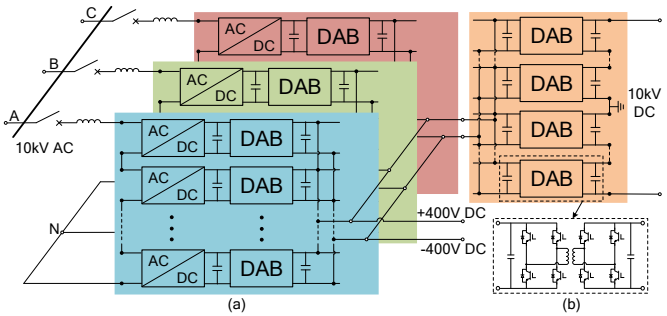

Fig. 1. Schematic diagram of PET: (a) Basic structure of PET; (b) Interior structure of DAB.

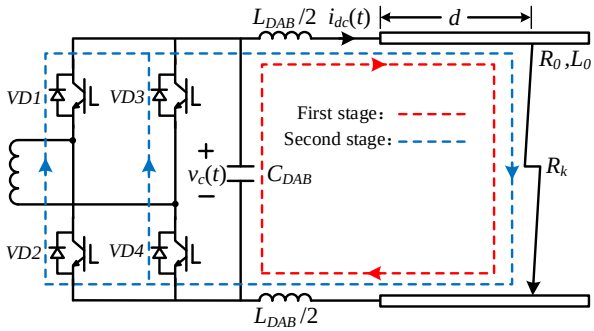

Fig. 2. Equivalent circuit of pole-to-pole fault.

of IGBTs are still under great threat during the fault, since they can function as the discharge path of short-circuit current.

The equivalent fault circuit modelled for fault characteristic analysis is shown in Fig. 2. Single DAB module is utilized to substitute cascaded DABs and this assumption works when equivalent parameters of cascaded DABs are used [24]. The terminal capacitor C_{DAB} gives voltage support and the inductor L_{DAB} is installed at the DC port as the smoothing filter and fault current limiter. R_0 and L_0 are unit parameters of DC lines. Grounding capacitors of π-model DC lines are neglected in deducing process for simplicity, but they are considered in simulation models. What's more, d reflects the fault distance between PET terminal and faulted point of the DC line. R_k represents fault resistance.

The transient processes of pole-to-pole faults can be divided into two main stages: RLC resonance stage and inductor current freewheeling stage. Different from fault characteristic with VSC, infeed current from the AC grid does not exist in short-circuit current with DAB terminal [22]. The expressions of terminal voltage $v_c(t)$ and short-circuit current $i_{dc}(t)$ are deduced in two stages and vital factors influencing fault characteristics are discussed.

1) RLC resonance stage

As shown in Fig. 2, typical RLC resonance occurs in the equivalent circuit when fault occurs. In this stage, the inductors in the circuit absorb energy from the discharging capacitor until the capacitor voltage drops to zero. The two order equation of this stage is expressed as:

$$L_{\Sigma}C_{DAB}\frac{d^2v_c(t)}{dt^2}+R_{\Sigma}C_{DAB}\frac{dv_c(t)}{dt}+v_c(t)=0 \qquad (1)$$

where $R_{\Sigma}=R_k+dR_0$, $L_{\Sigma}=L_{DAB}+dL_0$. It is worthy of mentioning that fault resistance in pole-to-pole fault has a small value. Hence, the critical condition

0885-8977 (c) 2018 IEEE. Personal use is permitted, but republication/redistribution requires IEEE permission. See http://www.ieee.org/publications_standards/publications/rights/index.html for more information.

This article has been accepted for publication in a future issue of this journal, but has not been fully edited. Content may change prior to final publication. Citation information: DOI 10.1109/TPWRD.2018.2867851, IEEE Transactions on Power Delivery

$$R_{\Sigma} < 2\sqrt{\frac{L_{\Sigma}}{C_{DAB}}} \tag{2}$$

is normally satisfied, in which fault circuit functions in underdamping resonance. Assuming the fault occurs when the time equals to 0, the expressions of terminal voltage and short-circuit current with the initial states of $v_c(0^+) = V_c$ and $i_{dc}(0^+) = I_{dc}$ are shown as:

$$v_c(t) = \frac{V_c\omega_0}{\omega_d} e^{-\alpha t}\cos(\omega_d t - \theta) - \frac{I_{dc}}{\omega_d C_{DAB}} e^{-\alpha t}\sin(\omega_d t) \tag{3}$$

$$i_{dc}(t) = \frac{V_c}{\omega_d L_{\Sigma}} \mathrm{e}^{-\alpha t}\sin(\omega_d t) + \frac{I_{dc}\omega_0}{\omega_d} \mathrm{e}^{-\alpha t}\cos(\omega_d t + \theta) \tag{4}$$

where $\alpha = R_{\Sigma}/(2L_{\Sigma}), \omega_0 = 1/\sqrt{L_{\Sigma}C_{DAB}}, \omega_d = \sqrt{\omega_0^2 - \alpha^2}$, and $\theta = \arctan(\alpha/\omega_d)$. As shown in (3), the terminal capacitor discharges drastically until its voltage drops to zero. The critical time between this two stages can be deduced from (3):

$$t_1 = \begin{cases} \dfrac{1}{\omega_d}\arctan\theta_L, & \theta_L \geq 0 \\ \dfrac{1}{\omega_d}\arctan\theta_L + \dfrac{\pi}{\omega_d}, & \theta_L < 0 \end{cases} \tag{5}$$

where $\theta_L = (\omega_d V_c C_{\mathrm{DAB}})/(I_{dc} - \alpha V_c C_{\mathrm{DAB}})$ .According to (5), the existence of load current impacts on the duration time of this stage. The duration time will be extended with load current flowing into DC port and vice versa.

2) Inductor current freewheeling stage

When zero crossing point of terminal voltage appears, the short-circuit current is allowed to flow through the anti-parallel diodes of IGBTs, which symbolizes the beginning of inductor current freewheeling stage. As shown in Fig. 2, the terminal capacitor is blocked by inverse voltage and short-circuit current attenuates with the time constant of RL circuit in this stage. The expressions of terminal voltage and short-circuit current in this stage are shown as:

$$v_c(t) = -R_{vd} I_{dc1} e^{-\frac{R_{vd}+R_{\Sigma}}{L_{\Sigma}}(t-t_1)} \tag{6}$$

$$i_{dc}(t) = I_{dc1} e^{-\frac{R_{vd}+R_{\Sigma}}{L_{\Sigma}}(t-t_1)} \tag{7}$$

where R_{vd} denotes the on-resistance of single anti-parallel diode and I_{dc1} denotes the critical short-circuit current which is the peak current appears in second stage.

Considering that diodes in the fault side H-bridges are completely exposed to short-circuit current and large current may cause breakdowns of diodes, breaker or fault current limiter installed at the terminal of DC port should be triggered during the RLC resonance stage and block diodes from the external faults in time.

3) Influence of fault distance and fault resistance

The expressions of terminal voltage and short-circuit current in two stages are deduced based on the assumption of short fault distance and negligible fault resistance. This assumption is valid only when (2) is satisfied. When fault distance d or fault resistance R_k keeps increasing, the relationship changes into

$$R_k > 2\sqrt{\frac{L_{DAB} + dL_0}{C_{DAB}}} - dR_0 \tag{8}$$

In this condition, overdamping property is presented in fault characteristics of pole-to-pole fault. The corresponding expressions of terminal voltage and short-circuit current are shown as:

$$v_c(t) = \frac{V_c}{s_2 - s_1}(s_2 e^{s_1 t} - s_1 e^{s_2 t}) + \frac{I_{dc}}{C_{DAB}(s_2 - s_1)}(e^{s_1 t} - e^{s_2 t}) \tag{9}$$

$$i_{dc}(t) = \frac{V_c C_{\mathrm{DAB}} s_1 s_2}{s_2 - s_1}(e^{s_2 t} - e^{s_1 t}) + \frac{I_{dc}}{s_2 - s_1}(s_2 e^{s_2 t} - s_1 e^{s_1 t}) \tag{10}$$

where $s_{1,2} = -\alpha \pm \sqrt{\alpha^2 - \omega_0^2}$.

C. Pole-to-ground Fault of DC Line

Fault characteristics of pole-to-ground fault are tightly related to grounding points in DC systems. For safety consideration, neutral point directly earth is commonly used in distribution network, in which fault characteristics of pole-to-ground fault are obvious and easy to be detected. Sometimes small grounding resistance is also applied to restrain maximum short-circuit current occurring in pole-to-ground faults [6]. Solid earth connection is used in this paper to evaluate the most serious condition. Thanks to the medium frequency transformers in DAB blocks, two ports of modular DAB blocks can realize electrical isolation. Hence, when pole-to-ground fault occurs in the external lines of DC port, the fault characteristics are typical RLC resonance and only related to the grounding point of terminal capacitors in fault side H-bridges. Considering that explicit discussions about RLC resonance have been given in fault analysis of pole-to-pole fault, the expressions of terminal voltage and short-circuit current in faulted cable will not be repeated. In the following paper, P-G fault represents positive-pole-to-ground fault and N-G fault relatively represents negative-pole-to-ground fault.

III. Principle of Fault Location Method

Fault characteristics and influence factors of DC line faults with DAB structure have been discussed and expressions of terminal current and short-circuit current in different conditions are deduced. Based on fault characteristics mentioned in Section II, this paper proposes a fault location method, which realizes precise fault location with short time window and suitable sampling frequency.

A. Definition of Ratio of Transient Voltage (ROTV)

As shown in Fig. 3, the ratio of DC-link voltage $v_{dc}(t)$ and terminal voltage $v_c(t)$ is defined as the ratio of transient voltage (*ROTV*) in time domain:

$$ROTV(t) = \frac{v_{dc}(t)}{v_c(t)} \tag{11}$$

In the normal condition, the load current that flows through the terminal inductor is constant and the voltages measured at both sides of the inductor equal to the rated voltage, which means *ROTV* is close to 1. While when DC fault occurs in the DC line, *ROTV* changes with the transient stage. Taking pole-to-pole fault for example, the dynamic response of *ROTV*

0885-8977 (c) 2018 IEEE. Personal use is permitted, but republication/redistribution requires IEEE permission. See http://www.ieee.org/publications_standards/publications/rights/index.html for more information.

This article has been accepted for publication in a future issue of this journal, but has not been fully edited. Content may change prior to final publication. Citation information: DOI 10.1109/TPWRD.2018.2867851, IEEE Transactions on Power Delivery

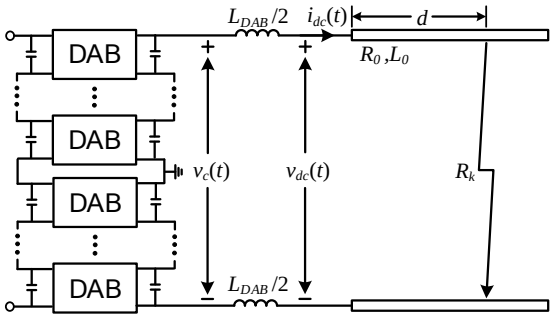

Fig. 3. Basic structure of DC lines with DAB terminal

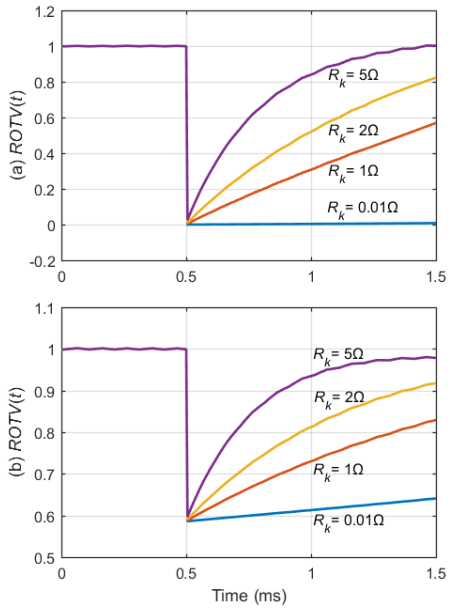

Fig. 4. *ROTVs* measured with different fault resistances and fault distances: (a) d = 0 km; (b) d = 10 km.

during the fault can be deduced from the equivalent circuit:

$$ROTV(t)=\frac{v_{dc}(t)}{v_c(t)}=\frac{v_c(t)-[v_c(t)-i_{dc}(t)R_\Sigma]\dfrac{L_{DAB}}{L_\Sigma}}{v_c(t)} \tag{12}$$

i.e.

$$ROTV(t)=\frac{dL_0}{L_\Sigma}+\frac{R_\Sigma L_{DAB}}{L_\Sigma}\frac{i_{dc}(t)}{v_c(t)} \tag{13}$$

The expression of *ROTV* can be divided into two components: the constant term and the time-variant term. The constant term relates to the fault distance apparently and the time-variant term is decided by short-circuit current $i_{dc}(t)$ and capacitor voltage $v_c(t)$. Since the precise expression of $i_{dc}(t)$ and v_c(t) can be obtained in Section II, the *ROTV* can be further deduced. It is worth mentioning that the magnitude of load current is negligible compared to the short-circuit current and damps fleetly after fault occurs, hence the terms related to load current in expressions of $i_{dc}(t)$ and $v_c(t)$ can be ignored. With respect to (3) and (4), the *ROTV* is represented as:

$$ROTV(t)=\frac{dL_0}{L_\Sigma}+\frac{R_\Sigma L_{DAB}}{L_\Sigma^2}\frac{1}{\omega_d\cot(\omega_d t)+\alpha} \tag{14}$$

According to the definition of *ROTV*, the time-variant term of *ROTV* is extremely close to zero after fault occurs and gradually increases with the fault process. The larger the fault resistance is, the faster this term increases. It means that *ROTV* always goes through a sudden dip after fault and the value that *ROTV* falls to is only correlated to fault distance.

Fig. 4 depicts *ROTVs* measured with different fault resistances at different fault locations. When fault distance d_1 is set as 0, the value of constant term also equals to 0. Consequently, no matter how fault resistances change, *ROTVs* always drop to 0 at the very beginning of fault in Fig. 4(a). When d_1 equals to 10 km, according to parameters in Table I, the constant term is close to 0.583 and fits the simulation results very well in Fig. 4(b).

The previous discussion seems to target at the pole-to-pole fault, but the obtained conclusion is also feasible for pole-to-ground fault. Since both of them go through RLC resonance stage after the fault occurs. When it comes to pole-to-ground fault, the definition of *ROTV* needs to be slightly modified as:

$$ROTV_j(t)=\frac{v_{dcj}(t)}{v_{cj}(t)}\quad j=p,n \tag{15}$$

where $v_{dcj}(t)$ and $v_{cj}(t)$ represent voltages to earth measured at two sides of terminal inductor and the character j refers to positive or negative pole. For the above reason, the following paper only focuses on the fault location method of the pole-to-pole fault without repeating the deducing process of pole-to-ground fault.

B. ROTV-Based Fault Location Method

According to the definition of *ROTV*, *ROTV* approaches to 1 in the normal condition and goes through sudden drop when fault occurs in its forward direction. What's more, *ROTV* reaches its minimum value (constant term) at the very beginning of fault and gradually recovers with fault process. Since constant term only relates to fault distance, a fault detection criterion can be designed according to this characteristic:

$$ROTV(t)\le\frac{DL_0}{L_{DAB}+DL_0} \tag{16}$$

where D relates to the total length of DC line. The term on the right side of (16) reflects the constant term of *ROTV* when fault is located at the remote end of DC line. Once (16) is satisfied, it means that fault locates somewhere in the range of DC line according to above discussion and *ROTV* after fault will be recorded and used for fault location. Considering that *ROTV* increases with large fault resistance, 1.2 times of actual length is used in (16) for redundancy. According to system parameters in Table I, the threshold is calculated as 0.63.

Since *ROTV* after fault can be obtained, the fault distance can be obtained by neglecting the time-variant term in (14). The measured fault distance is deduced as:

$$d=\frac{L_{DAB}}{L_0}\frac{ROTV}{1-ROTV} \tag{17}$$

where *ROTV* is defined as the mean value of first five signals measured after fault within time window. Fault distances can be calculated accurately in three kinds of faults on the condition of metallic fault or low-resistance fault. But with fault resistances increasing, the impact of time-variant term can not be ignored and the calculation errors of results enhance drastically. As a result, the accuracy of estimated

0885-8977 (c) 2018 IEEE. Personal use is permitted, but republication/redistribution requires IEEE permission. See http://www.ieee.org/publications_standards/publications/rights/index.html for more information.

This article has been accepted for publication in a future issue of this journal, but has not been fully edited. Content may change prior to final publication. Citation information: DOI 10.1109/TPWRD.2018.2867851, IEEE Transactions on Power Delivery

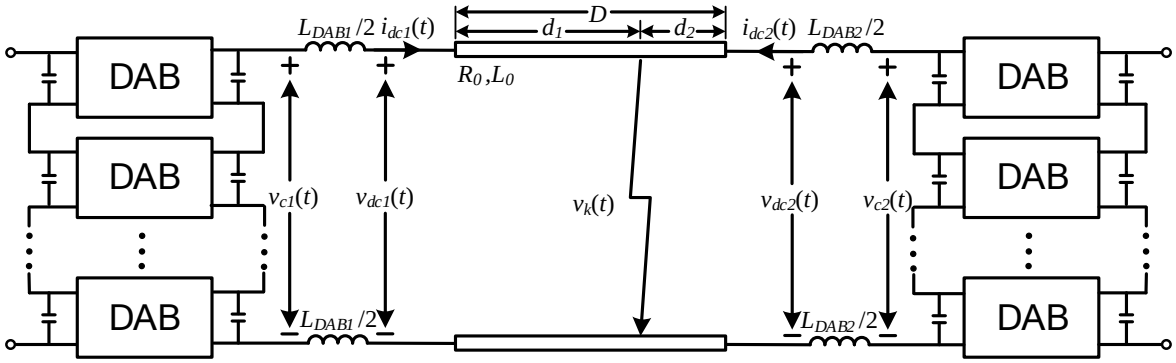

Fig. 5. Basic structure of two-terminal transmission system

fault distance based on single-terminal parameters is strictly restrained by fault resistance.

1) Fault location method with homogenous line

Considering the vulnerability of single-terminal fault location method, an improved fault location method based on *ROTVs* measured at two terminals is proposed. As shown in Fig. 5, DC ports of PET with same rated voltage can be connected with DC lines to realize power delivery. The basic structure shares similarities with VSC-based transmission system and modular DAB blocks are used to substitute VSCs at the terminal of DC lines. *ROTVs* measured in this structure can be defined as (13) similarly. However, it should be noticed that short-circuit currents flowing into faulted point come from both sides in this condition and *ROTVs* measured at two terminals are rewritten as:

$$ROTV_1(t)=\frac{d_1L_0}{L_{\Sigma1}}+\frac{L_{DAB1}}{L_{\Sigma1}}\frac{v_k(t)}{v_{c1}(t)}+\frac{d_1R_0L_{DAB1}}{L_{\Sigma1}}\frac{i_{dc1}(t)}{v_{c1}(t)} \tag{18}$$

$$ROTV_2(t)=\frac{d_2L_0}{L_{\Sigma2}}+\frac{L_{DAB2}}{L_{\Sigma2}}\frac{v_k(t)}{v_{c2}(t)}+\frac{d_2R_0L_{DAB2}}{L_{\Sigma2}}\frac{i_{dc2}(t)}{v_{c2}(t)} \tag{19}$$

where $v_k(t)$ represents the voltage of fault resistance and L_0 represents equivalent inductance of per km DC line. Notice that $i_{dc}(t)$ refers to inductor current and $v_c(t)$ refers to capacitor voltage, neither of them can mutate at the very beginning of fault, i.e.

$$\begin{cases} i_{dc1}(0^+)=i_{dc1}(0^-)=-i_{dc2}(0^+)=-i_{dc2}(0^-)=I_{dc} \\ v_{c1}(0^+)=v_{c1}(0^-)=v_{c2}(0^+)=v_{c2}(0^-)=V_c \end{cases} \tag{20}$$

Based on (20), the expressions of *ROTV* measured at two terminal can be combined to eliminate the $v_k(t)$ term to diminish the impact of fault resistance. The combinatorial term is shown as:

$$\frac{L_{\Sigma1}}{L_{DAB1}}ROTV_1(0^+)-\frac{L_{\Sigma2}}{L_{DAB2}}ROTV_2(0^+)= \frac{d_1L_0}{L_{DAB1}}-\frac{d_2L_0}{L_{DAB2}}+\frac{d_1R_0i_{dc1}(0^+)}{v_{c1}(0^+)}-\frac{d_2R_0i_{dc2}(0^+)}{v_{c2}(0^+)} \tag{21}$$

The last two terms in (22) can be further simplified as:

$$\frac{d_1R_0i_{dc1}(0^+)}{v_{c1}(0^+)}-\frac{d_2R_0i_{dc2}(0^+)}{v_{c2}(0^+)}=\frac{DR_0I_{dc}}{V_c} \tag{22}$$

The physical meaning of this term is ratio of the voltage drop in DC transmission line and the rated voltage during the normal condition, which is normally negligible. So it is reasonable to neglect this term to simplify the equation deduction. The only unknown parameter in the left terms of (21) is the fault distance d_1 (d_2 can be replaced by D-d_1), so the fault distance d_1 can be expressed as:

$$d_1=\frac{L_{DAB1}L_{DAB2}(ROTV_1-ROTV_2)+DL_0L_{DAB1}(1-ROTV_2)}{L_0L_{DAB2}(1-ROTV_1)+L_0L_{DAB1}(1-ROTV_2)} \tag{23}$$

Specially, if the inductors installed at two terminals have same value, the (23) can be simplified as:

$$d_1=\frac{L_{DAB}(ROTV_1-ROTV_2)+DL_0(1-ROTV_2)}{L_0(1-ROTV_1)+L_0(1-ROTV_2)} \tag{24}$$

As shown in (23), the fault distance depends on *ROTVs* measured at two terminals and parameters of terminal inductors and DC lines. Considering that parameters of terminal inductors and DC lines are already known before the fault, *ROTVs* are the only parameters needed to measure after the fault and the process of fault location is completely simplified.

2) Fault location method with mixed lines

In the previous discussion, the cable between two terminals is considered with homogenous parameters. In practical engineering application, sometimes cables are mixed with overhead lines to realize power delivery in distribution network. To apply proposed fault location method in mixed lines with different parameters, mixed lines should be replaced by the equivalent homogenous line.

According to (23), fault location method has a strong relationship with inductor of line model but has a weak relationship with resistance. Hence, the impact of line resistance is neglected. Fig. 6 depicts equivalent line model of mixed lines with different parameters, where L_1 and L_2 represents unit inductor of line 1 and line 2 and d^* denotes the length of line 1. In the equivalent model, line 2 is transferred to the line with unit inductor of line 1. It can be seen that the equivalent model has same line inductor with mixed lines. The length of equivalent line is shown as

$$D'=d^*+\frac{L_2}{L_1}(D-d^*) \tag{25}$$

Since equivalent line is homogenous, fault distance in equivalent model can be calculated by:

$$d_1'=\frac{L_{DAB1}L_{DAB2}(ROTV_1-ROTV_2)+D'L_1L_{DAB1}(1-ROTV_2)}{L_1L_{DAB2}(1-ROTV_1)+L_1L_{DAB1}(1-ROTV_2)} \tag{26}$$

0885-8977 (c) 2018 IEEE. Personal use is permitted, but republication/redistribution requires IEEE permission. See http://www.ieee.org/publications_standards/publications/rights/index.html for more information.

This article has been accepted for publication in a future issue of this journal, but has not been fully edited. Content may change prior to final publication. Citation information: DOI 10.1109/TPWRD.2018.2867851, IEEE Transactions on Power Delivery

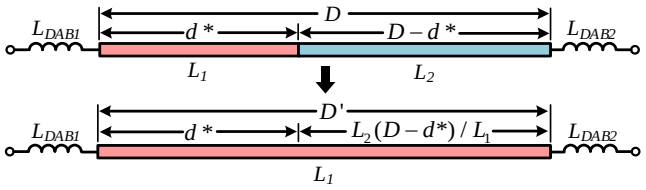

Fig. 6. Equivalent line model of mixed lines with different parameters

TABLE I
Simulation Parameters of System

Parameters	Value
V_c	10 kV
I_{dc}	0.1kA
C_{DAB}	250 uF
L_{DAB}	2 mH
R_0	0.06 Ω/km
L_0	0.28 mH/km
C_0	20 pF/km
D	10 km

It should be noted that fault distance obtained from (26) does not equal to actual value, except that estimated distance is smaller than d^*. Since the length of line 2 is transferred, actual fault distance should be changed with respect to convert coefficient when estimated distance d_1' is larger than d^*. Actual fault distance is calculated as follows:

$$d_1 = \begin{cases} d_1' & d_1' \le d^* \\ \dfrac{L_1}{L_2} d_1' + \dfrac{L_2 - L_1}{L_2} d^* & d_1' > d^* \end{cases} \quad (27)$$

IV. Simulation and Discussions

The two-terminal fault location method based on *ROTV* is proposed to solve the problem of fault resistance, which is the main shortcoming of single-terminal fault location method. In this section, this improved method is tested under different fault types, fault locations and fault resistances to evaluate the endurance to fault resistance under various conditions. The considerable factors that influence the performance of fault location method such as sampling frequency, time window and operating condition will be further discussed.

A. System parameters and fault characteristics

To verify the validity of fault characteristic analysis in Section II, simulations of P-N fault are operated in the external DC line of 10kV DC port. The configuration of single terminal model can be obtained in Fig. 3 and simulation parameters are listed in Table I, where equivalent parameters of cascaded DABs are used.

1) P-N fault with small fault resistance

The transient responses of pole-to-pole fault with small fault resistance are depicted in Fig. 7, where fault distance is set as 2 km and fault resistance is equal to 1 Ω. The expressions of terminal voltage and short-circuit current obtained according to two-stage analytic process are proved to be almost as same as the simulated results. As shown in Fig. 7(a), the terminal capacitor discharges until its terminal voltage drops to zero. The critical time occurs when t = 1.4 ms in Fig. 7(b) and the critical current I_{dc1} is about 2.29 kA which turns out to be the maximum current in second stage. Short-circuit current keeps damping in second stage and eventually vanishes when t = 8 ms.

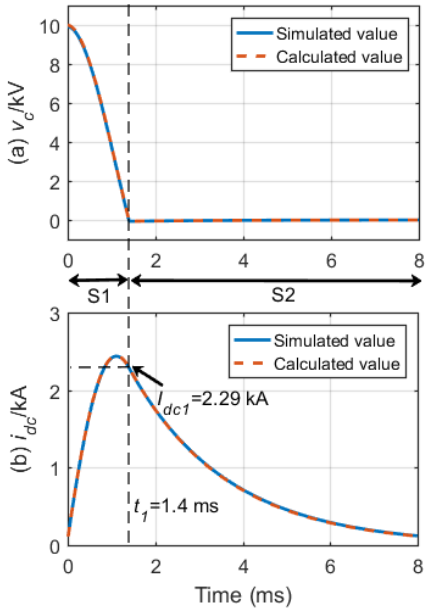

Fig. 7. Fault characteristics of pole-to-pole fault (R_k=1 Ω): (a) Waveforms of terminal voltage; (b) Waveforms of short-circuit current.

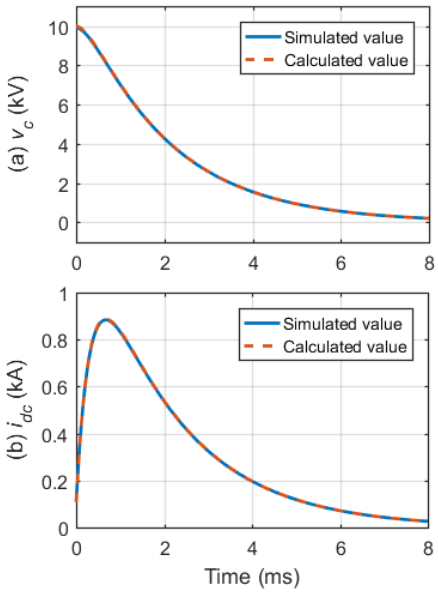

Fig. 8. Fault characteristics of pole-to-pole fault (Rk =10 Ω): (a) Waveforms of terminal voltage; (b) Waveforms of short-circuit current.

2) P-N fault with large fault resistance

Fig. 8 shows fault characteristics of high-resistance pole-to-pole fault. Fault distance is set as 2 km and fault resistance is equal to 10 Ω. In this condition, (7) is satisfied and only RLC resonance stage occurs after the fault. It should be noted that the impact of load resistance (equals to 100 Ω) in external circuit can no longer be neglected when fault resistance is large. The load resistance diminishes the equivalent fault resistance and relatively increases current peak, which is not considered in theoretical derivation. With load resistance considered, the calculated results match with results obtained from the simulation very well. It can be seen that terminal voltage damps in similar pace with short-circuit current during the whole process in Fig. 8(a), which is completely different from that in low-resistance fault. As shown in Fig. 8(b), current peak is much lower in high-resistance fault.

0885-8977 (c) 2018 IEEE. Personal use is permitted, but republication/redistribution requires IEEE permission. See http://www.ieee.org/publications_standards/publications/rights/index.html for more information.

This article has been accepted for publication in a future issue of this journal, but has not been fully edited. Content may change prior to final publication. Citation information: DOI 10.1109/TPWRD.2018.2867851, IEEE Transactions on Power Delivery

TABLE II
ESTIMATED FAULT DISTANCES AND *ERS* IN POLE-TO-POLE FAULT

$d_{1.act}$/km	Results	Fault Resistance 0.01Ω	1Ω	2Ω	5Ω
0	$d_{1.est}$/km	-0.0054	-0.0057	-0.0060	-0.0070
	ER/%	0.054	0.057	0.060	0.070
2.5	$d_{1.est}$/km	2.5155	2.5154	2.5153	2.5150
	ER/%	0.155	0.154	0.153	0.150
5	$d_{1.est}$/km	5.0366	5.0337	5.0338	5.0356
	ER/%	0.366	0.337	0.338	0.356
7.5	$d_{1.est}$/km	7.5486	7.5489	7.5491	7.5509
	ER/%	0.486	0.489	0.491	0.509
10	$d_{1.est}$/km	10.0610	10.0614	10.0619	10.0624
	ER/%	0.610	0.614	0.619	0.624

TABLE III
ESTIMATED FAULT DISTANCES AND *ERS* IN POLE-TO-GROUND FAULT

$d_{1.act}$/km	Fault Type	Results	Fault Resistance 1Ω	20Ω	50Ω	100Ω
0	P-G	$d_{1.est}$/km	0.0001	-0.0208	-0.0428	-0.0677
		ER/%	0.001	0.208	0.428	0.677
	N-G	$d_{1.est}$/km	0.0002	-0.0184	-0.0270	-0.0362
		ER/%	0.002	0.184	0.270	0.362
2.5	P-G	$d_{1.est}$/km	2.5203	2.5094	2.5012	2.5177
		ER/%	0.203	0.094	0.012	0.177
	N-G	$d_{1.est}$/km	2.5202	2.5094	2.4992	2.4935
		ER/%	0.202	0.094	0.008	0.065
5	P-G	$d_{1.est}$/km	5.0367	5.0287	5.0225	5.0229
		ER/%	0.367	0.0287	0.225	0.229
	N-G	$d_{1.est}$/km	5.0368	5.0286	5.0204	5.0162
		ER/%	0.368	0.286	0.204	0.162
7.5	P-G	$d_{1.est}$/km	7.5500	7.5401	7.5239	7.5036
		ER/%	0.500	0.401	0.239	0.036
	N-G	$d_{1.est}$/km	7.5499	7.5419	7.5326	7.5259
		ER/%	0.499	0.419	0.326	0.259
10	P-G	$d_{1.est}$/km	10.0600	10.0508	10.0356	10.0168
		ER/%	0.600	0.508	0.356	0.168
	N-G	$d_{1.est}$/km	10.0602	10.0554	10.0486	10.0442
		ER/%	0.602	0.554	0.486	0.442

B. Estimated Fault Distances under Various Conditions

The aforementioned discussion proves that this improved fault location method eliminates the impact of fault resistance by utilizing *ROTVs* measured at two terminals in theory. To realize this method, voltage sensors should be installed at both sides of the terminal inductors. These sensors measure voltages simultaneously by using the same sampling signal and the sampling frequency is set as 50 kHz. The two-terminal system configuration is reflected in Fig. 5 and parameters of terminal inductors and DC lines are the same as before. And to give better evaluation to validity and accuracy of this method, the calculation error of estimated fault distances ought to be defined. In this paper, the error rate (*ER*) is expressed as:

$$ER=\left|\frac{d_{1,est}-d_{1,act}}{D}\right|\times 100\% \tag{28}$$

where $d_{1,est}$ denotes the estimated fault distance and $d_{1,act}$ denotes the actual fault distance.

1) Pole-to-pole fault

Considering that most of pole-to-pole faults are caused by physical damage, fault resistance between two cables is small. Hence, fault resistance considered in pole-to-pole fault is up to 5 ohms. The estimated fault distances and *ERs* using two-terminal *ROTV*-based fault location method with different fault distances and resistances are shown in Table II. Fault distances measured by this proposed method can precisely reflect the fault locations from Table II. The largest *ER* of estimated fault distances is merely 0.6%, which appears near another terminal of DC lines in P-N fault. It can be seen that with the fault distance increasing, increment in *ERs* is not obvious. According to basic principle of the two-terminal *ROTV*-based fault location method, the impact of fault resistance is eliminated theoretically, which is also supported by the simulation results.

TABLE IV
ESTIMATED FAULT DISTANCES AND *ERS* IN MIXED LINES (R_K= 1Ω)

Fault Type	Results	$d_{1.act}$/km 0	4	6	8	10
P-N	$d_{1.est}$/km	-0.0021	4.0422	6.0403	8.0470	10.0502
	ER/%	0.021	0.422	0.403	0.470	0.502
P-G	$d_{1.est}$/km	0.0047	4.0459	6.0419	8.0475	10.0494
	ER/%	0.047	0.459	0.419	0.475	0.494
N-G	$d_{1.est}$/km	0.0056	4.0468	6.0427	8.0483	10.0503
	ER/%	0.056	0.468	0.427	0.483	0.503

2) Pole-to-ground fault

There are many reasons accounting for the occurrence of pole-to-ground fault, such as environmental stress, electrical stress and insulation aging, which means fault resistance in pole-to-pole fault varies in a wide range [22]. Considering this reason, pole-to-ground faults with fault resistances ranging from 1 Ω to 100 Ω are simulated. The estimated fault distances and *ERs* are displayed in Table III. Similar to pole-to-pole fault, this proposed method has an outstanding performance in pole-to-ground fault with small fault resistances. *ERs* of estimated distances are still acceptable with fault resistance increasing, which means increasing fault resistances have no direct connection with *ERs* of estimated fault distances. What's more, the estimated distances have no obvious difference between P-G and N-G faults with same fault condition.

3) Mixed line

In the above discussion, proposed method is tested in DC line with homogenous parameter. In this part, performance of fault location method will be evaluated in mixed lines, which shares the same structure in Fig. 6. In the simulation model, *D* is still 10 km and *d** is set as 6 km. L_1 equals to 0.28 mH/km and L_2 equals to 0.42 mH/km. Other parameters can be obtained in Table I. According to (25), length of equivalent line is calculated as 12km. Simulation results with respect to mixed lines are listed in Table IV. It is observed that modified fault location method accurately reflects the fault distance in mixed lines. Fault location near the joint is paid special attention, which still shows a good performance.

C. Analysis of Influence Factors

1) Influence of asynchronous data

As is known to all, for fault location methods based on two-terminal parameters, the major problem causing the calculation error is that parameters measured at two terminals might be out of sync. Synchronization error can be eliminated by using high-performance GPS-based time synchronization at two terminals [25]. However, since two-terminal parameters are collected for calculation, the existence of communication delay and hardware delay also causes unavoidable error in data synchronization. Considering this problem, asynchronous

0885-8977 (c) 2018 IEEE. Personal use is permitted, but republication/redistribution requires IEEE permission. See http://www.ieee.org/publications_standards/publications/rights/index.html for more information.

This article has been accepted for publication in a future issue of this journal, but has not been fully edited. Content may change prior to final publication. Citation information: DOI 10.1109/TPWRD.2018.2867851, IEEE Transactions on Power Delivery

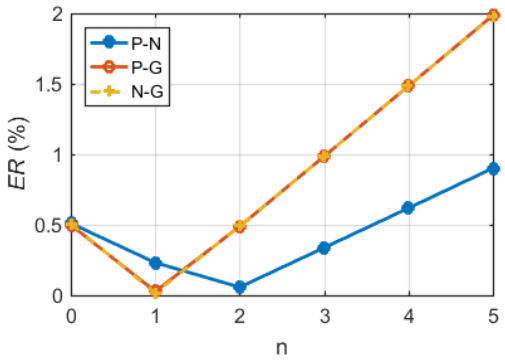

Fig. 9. *ERs* of fault distances calculated with asynchronous data

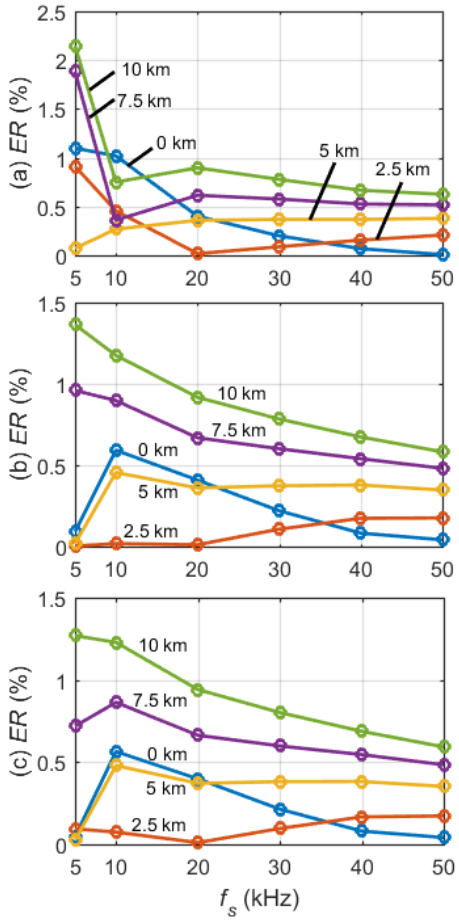

Fig. 10. The impact of sampling frequency on the estimated fault distances: (a) *ERs* in P-N fault; (b) *ERs* in P-G fault; (c) *ERs* in N-G fault.

data are used for simulation to evaluate the performance of proposed method. In the simulation, fault is located at 7.5 km and fault resistance is set as 5 Ω. Time delay causes data offset between parameters measured at two ends, and up to 5 offset points are considered.

Fig. 9 depicts *ERs* of fault distances calculated with data offset n. It is observed that calculation error grows with increasing offset points. Parameters in fault circuits differ in pole-to-pole fault and pole-to-ground fault, which accounts for different changing rates of *ERs*. However, variation tendencies of *ERs* are consistent for all three kinds of faults. According to sampling frequency, 5 offset points represent 0.1 ms in time delay. In this situation, maximum *ER* that occurs in pole-to-ground fault is around 2 %, which is still in the range of tolerance.

In worst situations, the existence of time delay will bring obvious influence to proposed method in online fault location mode. However, the time error between *ROTVs* measured at two terminals can be eliminated in offline mode. Considering that minimum value of *ROTV* appears in the beginning of fault, *ROTVs* measured at two terminals can be adjusted according to their minimum values in offline mode.

2) Influence of sampling frequency and time window

In the previous simulations, the sampling frequency is set as 50 kHz and the *ERs* of estimated fault distances are proved to be acceptable under various fault conditions. However, higher sampling frequency correlates to higher requirement for sampling hardware, higher cost and less feasibility. For this reason, the performance of this proposed method is evaluated under different sampling frequencies. According to the principle of the proposed method, this method relies on the transient information of line boundary. The transient process becomes shorter with fault resistance increasing, which means this method becomes more sensitive to sampling frequency with large fault resistance. Hence, the fault resistance is set as 5 Ω and sampling frequency ranges from 5 kHz to 50 kHz.

Fig. 10 shows *ERs* of estimated fault distances with different sampling frequencies in all three kinds of faults. As depicted in Fig. 10(a), *ERs* of fault distances measured at the same fault location decrease with sampling frequency in P-N fault. The maximum calculation error is around 2.2 % when sampling frequency is set as 5 kHz. *ERs* start to converge when sampling frequency is more than 20 kHz, which is restricted to the level of one percentage. Fig. 10(b) and Fig. 10(c) reflect the *ERs* appearing in pole-to-ground fault. It is observed that variation tendency of *ERs* has no obvious difference with that in P-N fault and the maximum calculation error is about 1.3 %. Since positive pole network is symmetric to negative pole network, characteristics of *ERs* with respect to sampling frequency are similar in P-G fault and N-G fault.

The simulation results prove that accuracy of proposed method will be influenced by sampling frequency, but fault distances estimated under 10 kHz are still acceptable. For higher location accuracy, higher sampling frequency is recommended.

As is mentioned above, first five *ROTVs* after fault are recorded to realize the fault location, which means the time window is flexible and relates to sampling frequency. If the sampling frequency ranges from 20 kHz to 50 kHz, the required time for sampling will range from 0.1 ms to 0.25 ms correspondingly. Hence, the time window set as 0.3ms is large enough for realizing this method.

3) Influence of operating conditions

Since the time window of this proposed method is much shorter than time that the terminal breaker needs to operate, the tripping operation of terminal break is impossible to influence the performance of this method. However, the operating condition of IGBTs in DABs is worthy of considering. IGBTs should be immediately blocked by fault detection (high current or low voltage) and the blocking time may conflict with the time window of this method. Unblocked IGBTs will enhance the short-circuit current and the *ROTVs* will be influenced. The estimated distances with blocked

0885-8977 (c) 2018 IEEE. Personal use is permitted, but republication/redistribution requires IEEE permission. See http://www.ieee.org/publications_standards/publications/rights/index.html for more information.

This article has been accepted for publication in a future issue of this journal, but has not been fully edited. Content may change prior to final publication. Citation information: DOI 10.1109/TPWRD.2018.2867851, IEEE Transactions on Power Delivery

TABLE V
ESTIMATED RESULTS UNDER DIFFERENT OPERATING CONDITIONS

$d_{1,act}$/km	*ROTV*s measured with Blocked IGBTs		*ROTV*s measured with unblocked IGBTs	
	$d_{1,est}$/km	ER/%	$d_{1,est}$/km	ER/%
0	-0.0070	0.070	0.0012	0.012
2.5	2.5150	0.150	2.5213	0.213
5	5.0356	0.356	5.0384	0.384
7.5	7.5509	0.509	7.5517	0.517
10	10.0624	0.624	10.0623	0.623

TABLE VI
ESTIMATED RESULTS WITH DIFFERENT GROUNDING RESISTANCES

Fault Type	Results	R_g/Ω				
		1	2	3	4	5
P-G	$d_{1.est}$/km	5.0382	5.0395	5.0405	5.0419	5.0430
	ER/%	0.382	0.395	0.405	0.419	0.430
N-G	$d_{1.est}$/km	5.0383	5.0394	5.0405	5.0417	5.0431
	ER/%	0.383	0.394	0.405	0.417	0.431

IGBTs and unblocked IGBTs are compared in P-N faults with 5 Ω fault resistance and the results are shown in Table V. It can be seen that this proposed method shows great performance whether IGBTs are blocked or not. The estimated distances have no obvious difference in two situations.

4) Influence of grounding resistance

As is mentioned above, grounding resistance will influence fault characteristic of pole-to-ground fault and relatively influence the accuracy of proposed method. Different from the neglected term (22) in P-N fault, this term in pole-to-ground fault should be modified as

$$\text{Neglected Term} = \frac{(DR_0 + 2R_{g1} + 2R_{g2})I_{dc}}{V_c} \tag{29}$$

where R_{g1} and R_{g2} represent grounding resistances at two terminals. They are installed in neutral points in Fig. 3.It is observed that this term is related to grounding faults in the system. Since this term is neglected in deducing process, the accuracy of proposed method will be influenced with grounding resistance increasing. In the previous simulation, grounding resistance is set as 0. Hence, small grounding resistances ranging from 1 to 5 Ω will be considered in metallic fault located at the middle point of the DC line.

Estimated results with different grounding resistances are listed in Table VI. The result shows that *ER*s slightly increase with grounding resistance increasing, which is in accordance with the conclusion obtained from (29). However, the impact of grounding resistance is not obvious when small grounding resistances are considered. In conclusion, the proposed method is promising in neutral point directly earth system and neutral point with small resistance system.

D. Comparison and Discussion

To further evaluate the performance of proposed method, we will compare our fault location method with previous methods in accuracy, speed and other aspects.

Probe current injection method proves to be efficient in fault location, especially in DC distribution network [19], [20]. The basic principle of this method is to inject signal current into the isolated fault zone with an additional probe power unit. The fault distance can be calculated according to natural response of signal current. Parameters of probe power unit are set according to mentioned papers and sampling frequency is set as 50 kHz for equity. This method will be compared to our proposed method in P-N fault with same system parameters.

TABLE VII
ESTIMATED RESULTS CALCULATED BY METHOD PROPOSED IN [20]

$d_{1.act}$/km	Results	Fault Resistance			
		0.01Ω	1Ω	2Ω	5Ω
0	$d_{1.est}$/km	0.0177	0.0177	0.1029	0.8061
	ER/%	0.177	0.177	1.029	8.061
2.5	$d_{1.est}$/km	2.5187	2.5187	2.6406	3.2293
	ER/%	0.187	0.187	1.406	7.293
5	$d_{1.est}$/km	4.9927	5.0423	5.1422	5.7553
	ER/%	0.073	0.423	1.422	7.553
7.5	$d_{1.est}$/km	7.5083	7.5659	7.6815	8.2695
	ER/%	0.083	0.659	1.815	7.695
10	$d_{1.est}$/km	10.0051	10.0695	10.1989	10.7891
	ER/%	0.051	0.695	1.989	7.891

Table VII displays estimated fault distances and *ER*s calculated by probe current injection method under different fault conditions and corresponding results of our method can be obtained in Table II. It can be seen that two methods are accurate enough when fault resistance is lower than 1 Ω. However, *ER*s of probe current injection method increase drastically with fault resistance growing. In contrast, *ER*s of proposed method is restricted to 0.6 % even when fault resistance equals to 5 Ω, which means our proposed method has an advantage in accuracy with high-resistance fault. What's more, both methods can realize fault location within 1 ms and satisfy the speed requirement. However, it should be noted that the accuracy of proposed method is based on four more voltage sensors and communication devices in two-terminal system, and only a simple hardware circuit is required in probe current injection method. Hence, probe current injection method proves to have a priority in cost.

Except for probe current injection method, travelling-wave-based method is proposed in [18]. Travelling-wave-based method can realize accurate fault location according to its basic principle. However, sampling frequency for this mothed is required to be at least 1 MHz considering that short length of DC line in distribution network. In comparison, proposed method can be realized in relatively low sampling frequency.

V. CONCLUSION

Fault characteristics of DC line faults are analyzed in detail with respect to DAB structure in this paper. PET is under great threat in the condition of pole-to-pole fault with metallic or low-resistance fault, where the fault process can be divided into RLC resonance stage and inductor current freewheeling stage. It is proved that diodes in fault side DABs are faced with breakdowns in the second stage and DC circuit breaker should operate in the first stage.

Considering the above restriction, the two-terminal *ROTV*-based fault location method proposed in this paper is capable of realizing accurate fault location for short DC lines with data only in the first stage, which means that time window has no conflict with the requirement of protection relaying. This proposed method is insensitive to fault distance and fault resistance with suitable sampling frequency, and proves to be feasible for homogenous and mixed lines in all three kinds of DC line faults. Furthermore, possible influence factors are

0885-8977 (c) 2018 IEEE. Personal use is permitted, but republication/redistribution requires IEEE permission. See http://www.ieee.org/publications_standards/publications/rights/index.html for more information.

This article has been accepted for publication in a future issue of this journal, but has not been fully edited. Content may change prior to final publication. Citation information: DOI 10.1109/TPWRD.2018.2867851, IEEE Transactions on Power Delivery

discussed in detail and accuracy of proposed method is verified to be acceptable. The proposed method has superiorities in accuracy and speed compared with other methods, especially in high-resistance faults, which is realized by additional voltage sensors and communication hardware.

In this paper, this method is discussed with respect to DC lines with two-terminal system. In the future work, the feasibility of proposed method will be discussed in multi-terminal system.

REFERENCE

[1] M. A. Perez, S. Bernet, J. Rodriguez, S. Kouro, and R. Lizana, "Circuit Topologies, Modeling, Control Schemes, and Applications of Modular Multilevel Converters," in *IEEE Transactions on Power Electronics*, vol. 30, no. 1, pp. 4-17, Jan. 2015.

[2] N. Flourentzou, V. G. Agelidis and G. D. Demetriades, "VSC-Based HVDC Power Transmission Systems: An Overview," in *IEEE Transactions on Power Electronics*, vol. 24, no. 3, pp. 592-602, March 2009.

[3] A. Q. Huang, M. L. Crow, G. T. Heydt, J. P. Zheng, and S. J. Dale, "The future renewable electric energy delivery and management (FREEDM) system: The energy Internet," in *Proceedings of the IEEE*, vol. 99, no. 1, pp. 133–148, Jan. 2011.

[4] S. Inoue and H. Akagi, "A bidirectional isolated DC–DC converter as a core circuit of the next-generation medium-voltage power conversion system," in *IEEE Transactions on Power Electronics*, vol. 22, no. 2, pp. 535–542, Mar. 2007.

[5] F. Blaabjerg and K. Ma, "Wind Energy Systems," in *Proceedings of the IEEE*, vol. 105, no. 11, pp. 2116-2131, Nov. 2017.

[6] T. Guillod, F. Krismer, and J. W. Kolar, "Protection of MV Converters in the Grid: The Case of MV/LV Solid-State Transformers," in *IEEE Journal of Emerging and Selected Topics in Power Electronics*, vol. 5, no. 1, pp. 393-408, March. 2017.

[7] S. Madhusoodhanan, D. Patel, S. Bhattacharya, J. A. Carr, and Z. Wang, "Protection of a transformerless intelligent power substation," *2013 4th IEEE International Symposium on Power Electronics for Distributed Generation Systems (PEDG)*, Rogers, AR, 2013, pp. 1-8.

[8] Z. Chen, *et al*. "Analysis and Experiments for IGBT, IEGT, and IGCT in Hybrid DC Circuit Breaker, " in *IEEE Transactions on Industrial Electronics*, vol. 65, no. 4, pp. 2883-2892, April 2018.

[9] P. Qiu, X. Huang, Y. Wang, Y. Lu, J. Chen, and F. Xu. "Application of High Voltage DC Circuit Breaker in Zhoushan VSC-HVDC Transmission Project," in *High Voltage Engineering*, vol. 44, no. 02, pp. 403-408, Feb. 2018.

[10] J. Yang, J. E. Fletcher, and J. O'Reilly, "Multiterminal DC Wind Farm Collection Grid Internal Fault Analysis and Protection Design," in *IEEE Transactions on Power Delivery*, vol. 25, no. 4, pp. 2308-2318, Oct. 2010.

[11] C. Fan, L. Liu, and Y. Tian, "A Fault-Location Method for 12-Phase Transmission Lines Based on Twelve-Sequence-Component Method," in *IEEE Transactions on Power Delivery*, vol. 26, no. 1, pp. 135-142, Jan. 2011.

[12] X. Yang, M. S. Choi, S. J. Lee, C. W. Ten, and S. I. Lim, "Fault Location for Underground Power Cable Using Distributed Parameter Approach," in *IEEE Transactions on Power Systems*, vol. 23, no. 4, pp. 1809-1816, Nov. 2008.

[13] M. Choi, S. Lee, D. Lee, and B. Jin, "A new fault location algorithm using direct circuit analysis for distribution systems," in *IEEE Transactions on Power Delivery*, vol. 19, no. 1, pp. 35-41, Jan. 2004.

[14] X. Lin, F. Zhao, G. Wu, Z. Li, and H. Weng, "Universal Wavefront Positioning Correction Method on Traveling-Wave-Based Fault-Location Algorithms," in *IEEE Transactions on Power Delivery*, vol. 27, no. 3, pp. 1601-1610, July 2012.

[15] R. J. Hamidi and H. Livani, "Traveling-Wave-Based Fault-Location Algorithm for Hybrid Multiterminal Circuits," in *IEEE Transactions on Power Delivery*, vol. 32, no. 1, pp. 135-144, Feb. 2017.

[16] J. Wu, H. Li, G. Wang, and Y. Liang, "An Improved Traveling-Wave Protection Scheme for LCC-HVDC Transmission Lines," in *IEEE Transactions on Power Delivery*, vol. 32, no. 1, pp. 106-116, Feb. 2017.

[17] L. Tang and B. T. Ooi, "Locating and Isolating DC Faults in Multi-Terminal DC Systems," in *IEEE Transactions on Power Delivery*, vol. 22, no. 3, pp. 1877-1884, July 2007.

[18] X. Chen, X. Yin, X. Yin, J. Tang and M. Wen, "A novel traveling wave based fault location scheme for power distribution grids with distributed generations," *2015 IEEE Power & Energy Society General Meeting*, Denver, CO, 2015, pp. 1-5.

[19] J. D. Park, J. Candelaria, L. Ma, and K. Dunn, "DC Ring-Bus Microgrid Fault Protection and Identification of Fault Location," in *IEEE Transactions on Power Delivery*, vol. 28, no. 4, pp. 2574-2584, Oct. 2013.

[20] R. Mohanty, U. S. M. Balaji and A. K. Pradhan, "An Accurate Noniterative Fault-Location Technique for Low-Voltage DC Microgrid," in *IEEE Transactions on Power Delivery*, vol. 31, no. 2, pp. 475-481, April 2016.

[21] X. Feng, L. Qi and J. Pan, "A Novel Fault Location Method and Algorithm for DC Distribution Protection," in *IEEE Transactions on Industry Applications*, vol. 53, no. 3, pp. 1834-1840, May-June 2017.

[22] J. Yang, J. E. Fletcher, and J. O'Reilly, "Short-Circuit and Ground Fault Analyses and Location in VSC-Based DC Network Cables," in *IEEE Transactions on Industrial Electronics*, vol. 59, no. 10, pp. 3827-3837, Oct. 2012.

[23] J. Liu, N. Tai and C. Fan, "Transient-Voltage-Based Protection Scheme for DC Line Faults in the Multiterminal VSC-HVDC System," in *IEEE Transactions on Power Delivery*, vol. 32, no. 3, pp. 1483-1494, June 2017.

[24] S. Jiang, C. Fan, N. Huang, and J. Zeng. "Fault Characteristic Analysis of DC Pole-to-Pole Fault in Power Electronic Transformer," in *Proceedings of the CSEE*, vol. 38, no. 05, pp. 1301-1309, Mar. 2018.

[25] Z. Li, T. Braun, and D. C. Dimitrova, "Methodology for GPS Synchronization Evaluation with High Accuracy," *2015 IEEE 81st Vehicular Technology Conference (VTC Spring)*, Glasgow, 2015, pp. 1-6.

Shan Jiang (S'18) received the B.S degree in electrical engineering and automation from Shanghai Jiao Tong University, Shanghai, China, in 2017. He is currently pursuing the M.S degree in electrical engineering from Shanghai Jiao Tong University, Shanghai, China.

His current research interests include the modelling, control and protection of AC-DC hybrid grid.

Chunju Fan received the B.S. degree in electrical engineering from Hefei University of Technology, Hefei, China, in 1990, and the M.S. degree in electrical engineering from Tianjin University, Tianjin, China, in 1993, and the Ph.D. degree in electrical engineering from Shanghai Jiao Tong University, Shanghai, in 2005. Currently, she is an associate professor of Electrical Engineering at Shanghai Jiao Tong University.

Her areas of interest are power system protection.

Ning Huang received the B.S degree in electrical engineering and automation from Shanghai Jiao Tong University, Shanghai, China, in 2017. He is currently pursuing the M.S degree in electrical engineering from Shanghai Jiao Tong University, Shanghai, China. His current research interests are AC and DC hybrid grid protection.

Ye Zhu received the B.S degree in electrical engineering and automation from Shanghai Jiao Tong University, Shanghai, China, in 2017. She is currently pursuing the M.S degree in electrical engineering from Shanghai Jiao Tong University, Shanghai, China. Her current research interests include power electronics and its reliability.

Muwei He is currently pursuing for the B.S degree in electrical engineering and automation from Shanghai Jiao Tong University, Shanghai, China. Her areas of interest are power system protection.

0885-8977 (c) 2018 IEEE. Personal use is permitted, but republication/redistribution requires IEEE permission. See http://www.ieee.org/publications_standards/publications/rights/index.html for more information.